Hetergeneous Catalysts Hot Paper

DOI: 10.1002/anie.201306863

Graphene-Supported Ultrafine Metal Nanoparticles Encapsulated by Mesoporous Silica: Robust Catalysts for Oxidation and Reduction Reactions**

Lu Shang, Tong Bian, Baihui Zhang, Donghui Zhang, Li-Zhu Wu, Chen-Ho Tung, Yadong Yin, and Tierui Zhang**

Abstract: *Graphene nanosheet-supported ultrafine metal nanoparticles encapsulated by thin mesoporous SiO_2 layers were prepared and used as robust catalysts with high catalytic activity and excellent high-temperature stability. The catalysts can be recycled and reused in many gas- and solution-phase reactions, and their high catalytic activity can be fully recovered by high-temperature regeneration, should they be deactivated by feedstock poisoning. In addition to the large surface area provided by the graphene support, the enhanced catalytic performance is also attributed to the mesoporous SiO_2 layers, which not only stabilize the ultrafine metal nanoparticles, but also prevent the aggregation of the graphene nanosheets. The synthetic strategy can be extended to other metals, such as Pd and Ru, for preparing robust catalysts for various reactions.*

Graphene has recently attracted tremendous attention, owing to its extraordinary electrical and thermal conductivity, excellent mechanical strength, unique optical and chemical properties, and a theoretical specific surface area of $2630\ m^2 g^{-1}$.[1] Compared to other carbon-based supports, such as graphite, activated carbon, and carbon nanotubes, graphene nanosheets have shown greatly enhanced catalytic activity in photocatalysis[2] and electrocatalysis;[3] this is mainly due to their excellent conductivity for electron capture and transport, the large specific surface area, and their unique interaction with catalyst particles.[4] High-efficiency thermocatalysis involving graphene-supported metal nanoparticles has also been investigated.[5] However, there are still a number of limitations to the practical application of most graphene-supported metal nanocatalysts. First, the strong π–π stacking interactions between graphene nanosheets can lead to serious aggregation and restacking, which inevitably blocks active catalytic sites, and thus significantly hampers the catalytic activity.[6] Second, general and robust methods for loading graphene nanosheets with ultrafine metal particles (< 2 nm), which promise significantly improved catalytic performance owing to their increased specific surface areas and high density of edges and corner atoms,[7] have been scarcely developed.[8] Third, owing to their high surface energy, metal nanoparticles are typically unstable and tend to sinter into larger species, especially under harsh reaction conditions such as at the high temperatures required for many catalytic reactions and subsequent detoxification processes, which results in a dramatic decrease in catalytic activity. To overcome these limitations, the dispersibility and stability of graphene-supported metal nanocatalysts must be improved by developing novel methods for anchoring ultrafine metal nanoparticles securely onto graphene supports.

Herein, we report a facile and scalable wet-chemical process to prepare graphene-nanosheet-supported metal nanoparticles covered by mesoporous silica ($mSiO_2$) layers. The amorphous and chemically and thermally stable $mSiO_2$ outer layer can restrain the π–π stacking interactions among graphene nanosheet supports and prevent the aggregation and restacking of graphene nanosheets. Additionally, a great number of mesopores in the $mSiO_2$ layers provide spaces for confining metal nanoparticles with specific sizes.[9] Moreover, the sintering of metal nanoparticles can be avoided, even under harsh reaction conditions, because of the confinement effects in porous materials.[10]

Scheme 1 illustrates the preparation process. Metal hydroxide (MOH), a precursor for metal nanoparticles, was first loaded onto the surface of graphene oxide (GO) nanosheets by a general deposition–precipitation method.[11] Subsequently, the residual ammonium hydroxide generated from the decomposition of urea was ingeniously used to catalyze the hydrolysis of tetraethyl orthosilicate (TEOS) directly to form a $mSiO_2$ shell covering the surface of MOH-GO composite. Cetyltrimethylammonium bromide (CTAB) was used as the pore-generating agent.[12] Lastly, the as-prepared nanosheets of MOH-GO@$mSiO_2$ were annealed under H_2, which converted GO into reduced graphene oxide (rGO) and

[*] Dr. L. Shang, T. Bian, B. H. Zhang, Dr. D. H. Zhang, Prof. L.-Z. Wu, Prof. C.-H. Tung, Prof. T. R. Zhang
Key Laboratory of Photochemical Conversion and Optoelectronic Materials, Technical Institute of Physics and Chemistry, Chinese Academy of Sciences, Beijing 100190 (P. R. China)
E-mail: tierui@mail.ipc.ac.cn
T. Bian, B. H. Zhang
University of Chinese Academy of Sciences
Beijing 100049 (P. R. China)
Prof. Y. Yin
Department of Chemistry, University of California
Riverside, CA 92521 (USA)
E-mail: yadong.yin@ucr.edu

[**] We acknowledge support from the Ministry of Science and Technology of China (2014CB239402, 2013CB834505), the National Natural Science Foundation of China (51322213, 20901081, 51172245, 91127005, 21201172), the Knowledge Innovation Project of the Chinese Academy of Sciences (KGCX2-EW-311-3), and the 100 Talents Program of the Chinese Academy of Sciences. Y.Y. also thanks the U.S. Department of Energy (DE-FG02-09ER16096) for financial support.

Supporting information for this article is available on the WWW under http://dx.doi.org/10.1002/anie.201306863.

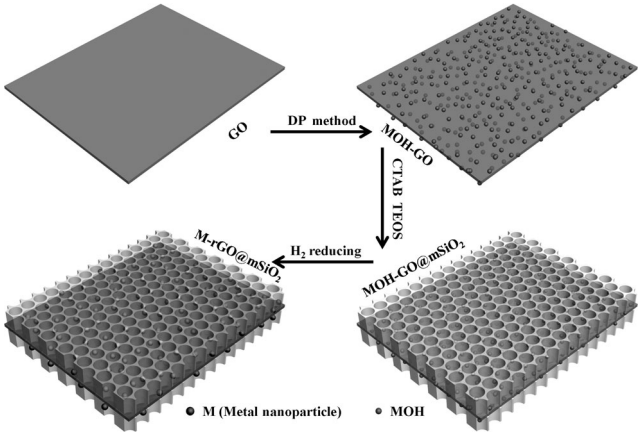

Scheme 1. Synthesis of M-rGO@mSiO$_2$.

MOH into metal nanoparticles, thus producing M-rGO@m-SiO$_2$ composite nanostructures.

As can be seen in representative scanning electron microscopy (SEM) images (Figure 1 a,b), Pt-rGO@mSiO$_2$ remains as a nanosheet-like structure, with lateral dimensions ranging from hundreds of nanometers to a few microns, and a thickness of approximately 28–30 nm. Loading catalyst nanoparticles into the sandwiched structures makes it convenient for recycling, compared to catalysts without supports.

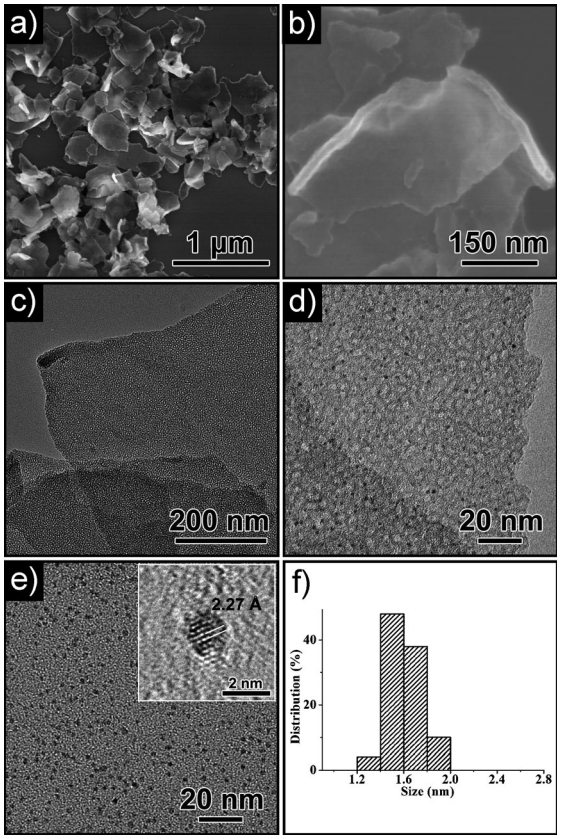

Figure 1. a,b) SEM images of Pt-rGO@mSiO$_2$. TEM images of c,d) Pt-rGO@mSiO$_2$ and e) Pt-rGO(etched). f) The size distribution of Pt nanoparticles in Pt-rGO@mSiO$_2$.

Further observation using transmission electron microscopy (TEM) indicates that mesopores with an average size of ca. 3 nm form uniformly in silica, whereas the Pt nanoparticles are well encapsulated between the rGO and mSiO$_2$ layers without any aggregation (Figure 1 c,d). The morphology of rGO and Pt nanoparticles can be more clearly observed after removing the outer mSiO$_2$ layers by etching with an aqueous solution of NaOH. As shown in Figure 1 e (see also the Supporting Information, Figure S1), uniform Pt nanoparticles with an average size of 1.65 nm are well dispersed on the rGO nanosheets. The high-resolution TEM image shows that the nanoparticles have a d spacing of 0.227 nm, which corresponds to the (111) plane of Pt (inset in Figure 1 e). The mesoporous structure of SiO$_2$ layers was further confirmed by Brunauer–Emmett–Teller (BET) gas adsorption studies (Figure S2), which suggest a typical isotherm type-IV curve, an average Barrett–Joyner–Halenda (BJH) pore diameter of 2.8 nm, and a surface area of 1057 $m^2 g^{-1}$. The chemical composition and structure of Pt-rGO@mSiO$_2$ were further investigated by energy-dispersive X-ray spectroscopy (EDX), Raman spectroscopy, and X-ray photoelectron spectroscopy (XPS). The EDX analysis indicates that only C, Si, O, and Pt are detected in Pt-rGO@mSiO$_2$, and that there is no other impurity (Figure S3a). The structural change, before and after thermal reduction under H_2 atmosphere, of the GO sandwiched between two layers of mSiO$_2$ was examined by Raman spectroscopy. The intensity ratio of the I_D/I_G value of GO decreases from 0.86 to 0.78 after thermal reduction, which reflects the formation of more sp^2 domains from the conversion of sp^3 carbons after thermal reduction, which is usually observed during H_2 reduction of GO (Figure S4).[13] The reduction of GO can be further supported by XPS monitoring of the chemical states change of carbon atoms in GO before and after thermal reduction. As shown in Figure S3 b, the typical XPS peaks of GO at 284.6, 286.6, 287.7, and 288.9 eV can be assigned to C–C (graphite), C–O, C=O, and O=C–O bonds, respectively. As a comparison, the relative content of C–O, C=O, and O=C–O bonds decreases significantly after thermal reduction, thus indicating that GO has been reduced to rGO (Figure S3 c).[3b,5b] Additionally, the Pt(4f) XPS spectrum was also collected (Figure S3 d). The two typical peaks at 71.4 and 74.6 eV for Pt $4f_{7/2}$ and Pt $4f_{5/2}$, respectively, are characteristic for metallic Pt^0,[14] which agree well with the HRTEM result.

The above results suggest that the ultrafine Pt nanoparticles with an average size of ca. 1.65 nm in Pt-rGO@m-SiO$_2$, display excellent stability at 240 °C under H_2 atmosphere, which can be attributed to the protection afforded by the mSiO$_2$ layers. To confirm the effect of mSiO$_2$ layers, Pt-rGO without mSiO$_2$ was prepared under otherwise identical reaction conditions for comparison. The TEM image of Pt-rGO in Figure S5 reveals that the size distribution of Pt nanoparticles in Pt-rGO is much wider, and the sizes of most nanoparticles are larger than 2.5 nm. In this regard, the mSiO$_2$ layers play a critical role in controlling the size and distribution of Pt nanoparticles during the synthesis of Pt-rGO@mSiO$_2$, due to the confining effects of mesopores.[15] For a robust nanocatalyst with practical use, it is expected to be stable at even higher temperatures in air and other

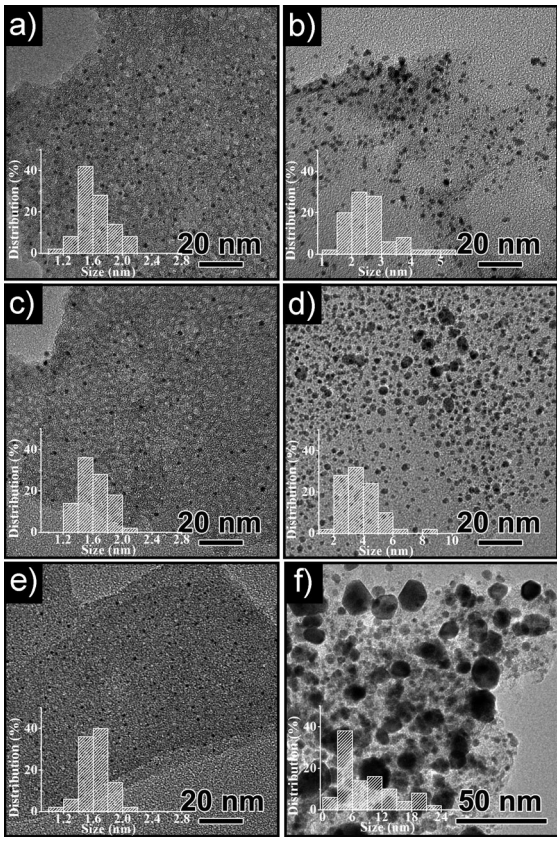

Figure 2. TEM images of Pt-rGO@mSiO$_2$ heat-treated at a) 300 °C in air, c) 500 °C in Ar, and e) 700 °C in Ar and Pt-rGO(etched) heat-treated at b) 300 °C in air, d) 500 °C in Ar, and f) 700 °C in Ar. All treatment times: 2 h.

atmosphere for various catalytic applications. Additional experiments were also carried out to test the thermal stability of Pt-rGO@mSiO$_2$ catalysts by calcining them at higher temperatures (300–700 °C; Figure 2). Figure 2 a,c,e show that the sizes of the Pt nanoparticles in Pt-rGO@mSiO$_2$ remain almost unchanged after calcination at 300 °C in air, and 500 °C and 700 °C in Ar (GO can be oxidized and decomposed in air at temperatures above 500 °C),[16] respectively, revealing that the as-prepared Pt-rGO@mSiO$_2$ nanocatalyst has superior thermal stability at temperatures as high as 700 °C. The same calcination experiments were also carried out on the comparison nanocatalyst Pt-rGO(etched), which lacks mSiO$_2$ protection layers. As can be seen in Figure 1 e, the sizes of the Pt nanoparticles in Pt-rGO(etched) increase to ca. 2.6 nm after calcination at 300 °C (Figure 2 b), to ca. 3.7 nm at 500 °C (Figure 2 d), and even to larger particles with sizes above 20 nm at 700 °C (Figure 2 f). This comparative study indicates that the mSiO$_2$ shell in Pt-rGO@mSiO$_2$ can effectively prevent the sintering of ultrafine Pt nanoparticles at high temperatures. Additionally, it should be noted that the graphene nanosheets act not only as a template with a large specific surface area to load a large amount of ultrafine Pt nanoparticles, but also as a space barrier (as do the mSiO$_2$ shells) to help prevent the sintering of ultrafine Pt nanoparticles at high temperatures. Heating the sample at even higher temperatures for 2 h, as shown in Figure S6, results in slight increases in Pt nanoparticle sizes from the original ca. 1.65 nm to 2.2 nm (800 °C) and 3.2 nm (850 °C). We attribute this size increase to the instability of the mSiO$_2$ wall under such high temperatures.[17] When graphene nanosheets are removed from Pt-rGO@mSiO$_2$ by calcination at 550 °C in air, as shown in Figure S7, the average size of ultrafine Pt nanoparticles increases to ca. 5.0 nm.

The catalytic performance of Pt-rGO@mSiO$_2$ was evaluated by employing the catalytic oxidation of CO as a model reaction.[18] Figure 3 shows the typical conversion ratio of CO

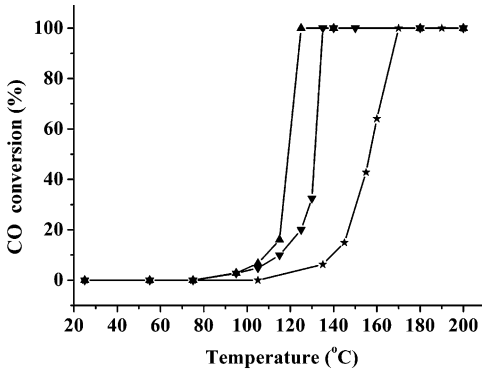

Figure 3. Catalytic activity of Pt-rGO@mSiO$_2$ post-calcined at 500 °C (▼) and 700 °C (▲) for CO oxidation. A sample without calcination (★) is also included for comparison.

as a function of reaction temperature over the Pt-rGO@mSiO$_2$ catalyst both with and without post-calcination treatment at 500 °C (Pt-rGO@mSiO$_2$-500) and 700 °C (Pt-rGO@mSiO$_2$-700) in Ar. Interestingly, Pt-rGO@mSiO$_2$ is not active at 105 °C, but Pt-rGO@mSiO$_2$-500 and Pt-rGO@mSiO$_2$-700 show a conversion ratio of 4.7 % and 6.8 %, respectively. The complete conversion of CO can be reached at 170 °C, 130 °C, and 120 °C for Pt-rGO@mSiO$_2$, Pt-rGO@mSiO$_2$-500, and Pt-rGO@mSiO$_2$-700, respectively. Evidently, with the increase of calcination temperature, the catalytic activity of the ultrafine Pt nanoparticles improves remarkably, which is possibly due to the removal of residual impurities on the surface of the Pt nanoparticles at higher calcination temperatures. Moreover, as shown in Table S1, the ignition temperature of Pt-rGO@mSiO$_2$-700 is lower than for some previously reported mSiO$_2$-based catalysts, such as Pt/SBA-15[19] and Pt@mSiO$_2$,[10a] and ultrafine Pt nanoparticles loaded on CeO$_2$, which is considered to be an active oxide support;[18] this reveals that both the ultrafine size of Pt and the graphene support could play key roles in the enhanced activity.[4a] Furthermore, the water–gas shift reaction (WGS) was chosen to test the high-temperature stability of Pt-rGO@mSiO$_2$. As shown in Figure S8, after an initial self-activation process, the CO conversion for the WGS reaction over Pt-rGO@mSiO$_2$ at 450 °C remained almost unchanged at ca. 30 % for about 80 h, thus demonstrating its excellent stability during high-temperature catalysis. This result is also consistent with stability studies involving heat-treatment and the CO oxidation reaction.

To demonstrate that our catalysts can also perform well in other reaction media, the catalytic performance of Pt-rGO@mSiO_2 in the liquid phase was investigated by employing the catalytic reduction of 4-nitrophenol (4-NP) in aqueous solution by hydrogen to produce 4-aminophenol (4-AMP) as a model reaction. The conversion of 4-NP can be readily monitored by UV/Vis photospectrometry, recording the change of its characteristic absorbance at $\lambda = 400$ nm in alkaline solution. As shown in Table 1, Pt-rGO@mSiO_2 gives complete conversion (100%) in 50 min, whereas within the same reaction time, Pt-rGO(etched) gives a conversion of only 87%, and Pt-rGO shows an even lower conversion of 25%, owing to the larger size and significant aggregation of the Pt nanoparticles (Figure S5). Compared with Pt-rGO-(etched), the higher catalytic activity of Pt-rGO@mSiO_2 is accounted for by the presence of the mSiO_2 layers. As mentioned before, the mSiO_2 layers can prevent the aggregation of rGO nanosheets and enhance their dispersion in the liquid phase (Figure S9) by weakening the π–π stacking interactions among rGO nanosheets dramatically, so that Pt nanoparticles in Pt-rGO@mSiO_2 expose more catalytic active sites in aqueous reaction systems for highly efficient catalytic conversion.

Table 1: Conversion of 4-NP over catalysts containing Pt nanoparticles.[a]

Entry	Catalyst	Conversion [%]
1	Pt-rGO@mSiO_2	100
2	Pt-rGO(etched)	87
3	Pt-rGO	25
4	poisoned Pt-rGO@mSiO_2[b]	16
5	regenerated Pt-rGO@mSiO_2[c]	100

[a] Reaction conditions: catalysts containing Pt nanoparticles (0.002 mmol), 4-NP (0.54 mmol), and H_2O (25 mL) were mixed and then reacted at 25 °C under H_2 (1 atm) for 50 min. [b] Pt-rGO@mSiO_2 was poisoned with MPA. [c] The poisoned Pt-rGO@mSiO_2 was calcined at 350 °C for 1 h in air.

In practical catalytic reactions, catalyst deactivation by feedstock poisoning occurs frequently. One of the most effective ways to regenerate the poisoned catalysts is high-temperature calcination. However, catalysts, especially nano-sized catalysts, can agglomerate and sinter very easily during high-temperature calcination owing to their high surface energy, even if they are anchored to the surface of supports.[17b,20] Because of the excellent thermal stability of Pt-rGO@mSiO_2 catalyst, it is expected to retain its high catalytic activity, even after the detoxification process. Sulfur species, such as H_2S, RSH, and RSSR, are common poisons for most metal-based catalysts because they block a great number of active sites by covering the catalyst surface through strong coordinate interaction. Mercaptopropionic acid (MPA) was thus chosen as a model poison for our tests. The regeneration behavior of Pt-rGO@mSiO_2 poisoned with MPA was studied under high-temperature calcination conditions. As indicated in Table 1, entry 3, the poisoned catalyst gives a very low (16%) conversion of 4-NP in 50 min. However, after calcination at 350 °C in air, the poisoned catalyst can be easily and completely regenerated, regaining 100% catalytic conversion (Table 1, entry 4).

Recycling and reusability are also important merits of robust heterogeneous catalysts. Typically, nanoparticle-based heterogeneous catalysts suffer from both low separation efficiency from reaction system, owing to their overall small size, and reduced catalytic activity caused by coagulation of nanoparticles during reactions. The micrometer-sized multilayer structure of the Pt-rGO@mSiO_2 nanocomposite is designed to overcome these challenges. After four cycles of catalytic hydrogenation of 4-NP in water using Pt-rGO@m-SiO_2, the conversion efficiency remains at 87%, which is almost the same as that of first run (90%), indicating the outstanding recyclability of the catalyst (Figure 4). On the other hand, for Pt-rGO(etched) without mSiO_2 layers, the conversion efficiency is only 74% after the first run, and gradually decreases to as low as 23% after four runs, mainly due to the aggregation of Pt nanoparticles, as confirmed by TEM observation (Figure S10). A similar decay in activity has also been observed for Pt-rGO, and extensively reported for carbon-supported metal catalysts.[21]

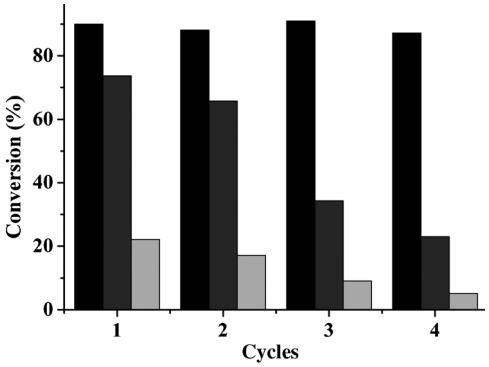

Figure 4. Recyclable catalytic reduction of 4-NP in water with Pt-rGO@mSiO_2 (black) and Pt-rGO(etched) (gray) and Pt-rGO (light gray). Reaction conditions: catalysts containing Pt nanoparticles (0.002 mmol), 4-NP (0.54 mmol), and H_2O (25 mL) were mixed and then reacted at 25 °C under H_2 (1 atm) for 40 min.

The facile synthetic route reported here is also general and can be extended to the preparation of Pd-rGO@mSiO_2 and Ru-rGO@mSiO_2 with structures similar to Pt-rGO@m-SiO_2 (Figure S11). Uniform ultrafine Pd and Ru nanoparticles with average particle sizes of 1.8 nm and 1.4 nm, respectively, well dispersed on rGO sheets, were sandwiched between two mSiO_2 layers. This generality means that this process has potential applications in a great number of catalytic reactions, such as hydrogenation, selective oxidations, and cross-coupling reactions.

In summary, we have developed a novel strategy for the facile preparation of graphene-nanosheet-supported ultrafine metal nanoparticles encapsulated by thin mSiO_2 layers. These robust catalysts show high catalytic activity, high stability under high temperature calcination, and excellent recycling and reusability in gas- and solution-phase reactions. In particular, the high activity of the catalyst can be fully recovered by high-temperature regeneration, in case they are

deactivated by feedstock poisoning. In addition to the high surface area provided by the graphene support, the enhanced catalytic performance is also attributed to the $mSiO_2$ layers, which not only provide an isolated and confined space for stabilizing the ultrafine metal nanoparticles, but also avoid aggregation among the graphene nanosheets by reducing their strong π–π stacking interactions. Furthermore, the synthetic strategy can be extended to other metals, such as Pd and Ru, to prepare graphene-supported ultrafine metal catalysts for various catalytic reactions,[22] or even multi-metal or alloy catalysts to improve the selectivity of industrially valuable catalytic reactions.[23]

Received: August 5, 2013
Published online: November 29, 2013

Keywords: graphene · heterogeneous catalysis · mesoporous materials · metal nanoparticles · stability

[1] a) K. S. Novoselov, A. K. Geim, S. V. Morozov, D. Jiang, Y. Zhang, S. V. Dubonos, I. V. Grigorieva, A. A. Firsov, *Science* **2004**, *306*, 666; b) C. N. R. Rao, A. K. Sood, K. S. Subrahmanyam, A. Govindaraj, *Angew. Chem.* **2009**, *121*, 7890; *Angew. Chem. Int. Ed.* **2009**, *48*, 7752; c) M. J. Allen, V. C. Tung, R. B. Kaner, *Chem. Rev.* **2009**, *109*, 132; d) X. Huang, X. Qi, F. Boey, H. Zhang, *Chem. Soc. Rev.* **2012**, *41*, 666.
[2] Q. Xiang, J. Yu, M. Jaroniec, *Chem. Soc. Rev.* **2012**, *41*, 782.
[3] a) Y. Liang, Y. Li, H. Wang, J. Zhou, J. Wang, T. Regier, H. Dai, *Nat. Mater.* **2011**, *10*, 780; b) Y. Li, H. Wang, L. Xie, Y. Liang, G. Hong, H. Dai, *J. Am. Chem. Soc.* **2011**, *133*, 7296; c) Y. Li, W. Gao, L. Ci, C. Wang, P. M. Ajayan, *Carbon* **2010**, *48*, 1124.
[4] a) E. Yoo, T. Okata, T. Akita, M. Kohyama, J. Nakamura, I. Honma, *Nano Lett.* **2009**, *9*, 2255; b) M. Zhou, A. Zhang, Z. Dai, C. Zhang, Y. P. Feng, *J. Chem. Phys.* **2010**, *132*, 194704.
[5] a) G. M. Scheuermann, L. Rumi, P. Steurer, W. Bannwarth, R. Mulhaupt, *J. Am. Chem. Soc.* **2009**, *131*, 8262; b) R. F. Nie, J. H. Wang, L. N. Wang, Y. Qin, P. Chen, Z. Y. Hou, *Carbon* **2012**, *50*, 586; c) B. F. Machado, P. Serp, *Catal. Sci. Technol.* **2012**, *2*, 54.
[6] P. V. Kamat, *J. Phys. Chem. Lett.* **2009**, *1*, 520.
[7] X. Chen, G. Wu, J. Chen, X. Chen, Z. Xie, X. Wang, *J. Am. Chem. Soc.* **2011**, *133*, 3693.
[8] H. Zhang, S. Chen, X. Quan, H. Yu, H. Zhao, *J. Mater. Chem.* **2011**, *21*, 12986.
[9] H. Zhu, B. Lee, S. Dai, S. H. Overbury, *Langmuir* **2003**, *19*, 3974.
[10] a) S. H. Joo, J. Y. Park, C. K. Tsung, Y. Yamada, P. Yang, G. A. Somorjai, *Nat. Mater.* **2009**, *8*, 126; b) Y. Dai, B. Lim, Y. Yang, C. M. Cobley, W. Li, E. C. Cho, B. Grayson, P. T. Fanson, C. T. Campbell, Y. Sun, Y. Xia, *Angew. Chem.* **2010**, *122*, 8341; *Angew. Chem. Int. Ed.* **2010**, *49*, 8165; c) Z. Sun, H. Zhang, Y. Zhao, C. Huang, R. Tao, Z. Liu, Z. Wu, *Langmuir* **2011**, *27*, 6244; d) I. Lee, Q. Zhang, J. Ge, Y. Yin, F. Zaera, *Nano Res.* **2011**, *4*, 115.
[11] a) B. Fang, N. K. Chaudhari, M. S. Kim, J. H. Kim, J. S. Yu, *J. Am. Chem. Soc.* **2009**, *131*, 15330; b) M. K. van der Lee, J. van Dillen, J. H. Bitter, K. P. de Jong, *J. Am. Chem. Soc.* **2005**, *127*, 13573.
[12] a) Q. Cai, Z. S. Luo, W. Q. Pang, Y. W. Fan, X. H. Chen, F. Z. Cui, *Chem. Mater.* **2001**, *13*, 258; b) S. B. Yang, X. L. Feng, L. Wang, K. Tang, J. Maier, K. Mullen, *Angew. Chem.* **2010**, *122*, 4905; *Angew. Chem. Int. Ed.* **2010**, *49*, 4795.
[13] S. H. Park, S. M. Bak, K. H. Kim, J. P. Jegal, S. I. Lee, J. Lee, K. B. Kim, *J. Mater. Chem.* **2011**, *21*, 680.
[14] B. G. Choi, H. S. Park, *ChemSusChem* **2012**, *5*, 709.
[15] a) Y. S. Chi, H. P. Lin, C. Y. Mou, *Appl. Catal. A* **2005**, *284*, 199; b) J. L. Gu, J. L. Shi, G. J. You, L. M. Xiong, S. X. Qian, Z. L. Hua, H. R. Chen, *Adv. Mater.* **2005**, *17*, 557; c) L. De Rogatis, M. Cargnello, V. Gombac, B. Lorenzut, T. Montini, P. Fornasiero, *ChemSusChem* **2010**, *3*, 24.
[16] Z. Wang, D. Xu, Y. Huang, Z. Wu, L. Wang, X. Zhang, *Chem. Commun.* **2012**, *48*, 976.
[17] a) M. T. Bore, H. N. Pham, E. E. Switzer, T. L. Ward, A. Fukuoka, A. K. Datye, *J. Phys. Chem. B* **2005**, *109*, 2873; b) T. W. Hansen, A. T. DeLaRiva, S. R. Challa, A. K. Datye, *Acc. Chem. Res.* **2013**, *46*, 1720.
[18] H. P. Zhou, H. S. Wu, J. Shen, A. X. Yin, L. D. Sun, C. H. Yan, *J. Am. Chem. Soc.* **2010**, *132*, 4998.
[19] J. Zhu, X. Xie, S. A. C. Carabineiro, P. B. Tavares, J. L. Figueiredo, R. Schomacker, A. Thomas, *Energy Environ. Sci.* **2011**, *4*, 2020.
[20] C. H. Bartholomew, *Appl. Catal. A* **2001**, *212*, 17.
[21] a) J. H. Vleeming, B. F. M. Kuster, G. B. Marin, F. Oudet, P. Courtine, *J. Catal.* **1997**, *166*, 148; b) C. E. Chan-Thaw, A. Villa, P. Katekomol, D. Su, A. Thomas, L. Prati, *Nano Lett.* **2010**, *10*, 537.
[22] Y. Tao, Y. Lin, Z. Huang, J. Ren, X. Qu, *Adv. Mater.* **2013**, *25*, 2594.
[23] a) D. Wang, Y. Li, *Adv. Mater.* **2011**, *23*, 1044; b) R. Ferrando, J. Jellinek, R. L. Johnston, *Chem. Rev.* **2008**, *108*, 845.

